Phys Chem Minerals (2006) 33: 17–27
DOI 10.1007/s00269-005-0035-0

ORIGINAL PAPER

Martin Kunz · George A. Lager · Hans-Beat Bürgi
Maria Teresa Fernandez-Diaz

High-temperature single-crystal neutron diffraction study of natural chondrodite

Received: 15 February 2005 / Accepted: 9 August 2005 / Published online: 5 January 2006

Abstract The H-atom environment in a Tilly Foster chondrodite was analyzed using single-crystal neutron-diffraction data collected at 500, 700 and 900 K and previously published low temperature data collected at 10, 100 and 300 K on the same crystal ($Mg_{4.64}Fe_{0.28}Mn_{0.014}Ti_{0.023}(Si_{1.01}O_4)_2F_{1.16}(OH)_{0.84}$; Friedrich et al. in Am Mineral 86:981–989, 2001). The full mean square displacement matrix Σ of the O–H pair was determined from the temperature dependence of the anisotropic displacement parameters, enabling a proper correction of the O–H bond for thermal vibration without assumptions about the correlation of O and H movements. The results show that the perpendicular O–H motions in chondrodite are intermediate between the riding and the independent motion models. The corrected O–H bond lengths do not change with temperature whereas the corrected H···F distances show an increase of ~0.02 Å with temperature, as do the Mg–O distances. This result shows that spectroscopic observations on the strength of the covalent O–H bond cannot be interpreted unambiguously in terms of a corresponding behaviour of the associated H···O/F hydrogen bond.

M. Kunz (✉)
Advanced Light Source, Lawrence Berkeley Laboratory,
1 Cyclotron Rd, MS 4R 0230, Berkeley, CA 94720, USA
E-mail: mkunz@lbl.gov
Tel.: +1-510-4952111

M. Kunz
Department of Earth and Planetary Science,
University of California, Berkeley, CA 94720, USA

G. A. Lager
Department of Geography and Geosciences,
University of Louisville, Louisville, KY 40292, USA

H.-B. Bürgi
Labor für chemische und mineralogische Kristallographie,
Universität Bern, CH-3012 Bern, Switzerland

M. T. Fernandez-Diaz
Institut Laue-Langevin, 38042 Grenoble, France

Keywords Chondrodite · Hydrous magnesium silicates · High temperature · Neutron diffraction · Hydrogen bonds · Anisotropic displacement parameters

Introduction

Exchange of fluid phases, namely water and CO_2, between the surface and the deep interior of the Earth is one of the interesting problems in modern earth science. Although it is well known that volcanic activities release large amounts of H_2O and CO_2, the amount of such gases that is recycled into the Earth's mantle is not well constrained. This uncertainty is mainly due to a strong dependence of the thermodynamic properties of minerals on the exact chemical composition of their volatile constituents, e.g. the OH/F ratio (Stalder and Ulmer 2001). Moreover, the volatile components can have a strong influence on the crystal structure and thus the physical properties and stability of a given mineral structure.

Chondrodite [$Mg_5Si_2O_8(F,OH)_2$] is a member of the family of humite minerals, a group of hydrous magnesium silicates with varying Mg_2SiO_4:$Mg(F,OH)_2$ ratio. All humite minerals are structurally closely related to forsterite (Mg_2SiO_4), which is regarded to be the most important mineral of the Earth's upper mantle. For this reason, humites are candidate materials for transporting significant amounts of fluid components, OH in particular, into the deep Earth. Chondrodite is of interest to us because it exhibits the large thermal stability necessary for such transport. Unlike other dense, hydrous Mg-silicates (DHMS), $(OH)_2$-chondrodite remains stable at ambient pressure up to 873 K. As suggested by Stalder and Ulmer (2001), its stability is enhanced by the substitution of half of the OH-groups by F as observed in most natural samples. Lager et al. (2001) argue that replacement of OH by F leads to stabilization by avoiding the occupation of a second hydrogen site, and the formation of additional hydrogen bonds with the oxygen sub-lattice, which weakens the metal–oxygen

bonds. The thermal stability of hydrous minerals and the behaviour of the O–H···O bond at high temperatures are relevant here, because dehydration is often the first break-down reaction of such minerals. Raman studies (Mernagh et al. 1999) of both OH- and F-bearing chondrodite show a slight decrease of the O–H vibrational frequency with increasing temperature. This is unusual when compared with other DHMS phases (Liu et al. 1997, 1998). It implies a decrease in the force-constant of the covalent O–H bond, which, in turn, suggests a lengthening of the O–H bond (Brown 2002). The increase of the covalent O–H bond length is expected to be paralleled by a decrease and thus strengthening of the hydrogen bond. Such a strengthening of the hydrogen-bond can have a decisive stabilizing influence on the crystal structure despite its relative weakness compared to ionic or covalent bonds (Hawthorne 1992).

In order to determine if the strengthening of the hydrogen bond in chondrodite, as suggested by spectroscopic measurements, could be detected by diffraction methods, we investigated a previously characterized (Friedrich et al. 2001, 2002) F-bearing chondrodite by single crystal neutron diffraction in the temperature range from 10 to 900 K. An F-bearing sample was chosen for study rather than a $(OH)_2$-chondrodite because single-crystals of the latter are not of sufficient size for neutron studies. Given the O/F disorder in this material, a special effort was made to determine the fractional coordinates and thermal parameters as accurately as possible. Particular attention was paid to two points: (1) the partial substitution of O by F, which implies two slightly different atomic positions and produces anomalously long O–H bonds if the disorder is not properly modelled; (2) the riding motion of the H atom, which causes an apparent shortening of the O–H bond at high temperatures.

Experimental and refinement details

We investigated a natural F-bearing chondrodite from the Tilly Foster Mine, Brewster, New York. Its chemical composition, $Mg_{4.64}Fe_{0.28}Mn_{0.014}Ti_{0.023}(Si_{1.01}O_4)_2F_{1.16}(OH)_{0.84}$), has been described by Friedrich et al. (2001). Accurate single-crystal neutron diffraction data were collected at three temperatures (500, 700, 900 K) on instrument D9 at the Institut Laue Langevin (ILL) in Grenoble at a wavelength of 0.8397(3) Å, selected with a Cu(220) monochromator in transmitting geometry (take-off angle = 38.4°). The same crystal had been used previously in a low-temperature (LT) single-crystal neutron diffraction study (10, 100, 295 K, HFIR, Oak Ridge National Laboratory; Friedrich et al. 2001). The sample was heated in a closed shell furnace capable of reaching temperatures up to 1,000 K. Reflections were recorded with a position sensitive detector consisting of 32×32 pixels. Detector to sample distance was 40 cm, which corresponds to a solid angle of 0.25°×0.25° (Lehmann et al. 1989). The data were integrated with a self-learned ellipsoid function (Wilkinson et al. 1988) and corrected for anisotropic absorption with program DATAP (Coppens et al. 1965). More details on data collection are given in Table 1.

While the ILL high temperature (HT) data were reduced to squares of the structure factor amplitudes (F^2), the Oak Ridge LT data were available only in the form of F. The reduced data were analyzed in space-group $P2_1/b$ (a unique) with the programs SHELXL-97 (Sheldrick 1997), and THMA11 (Schomaker and Trueblood 1998), as implemented in the package WinGX (Farrugia 1999). CrystalMaker (Palmer 2003) and XTALDRAW (Downs and Hall-Wallace 2003) were used to compute bond-distances and displacement probability ellipsoids. To ensure reliable and consistent atomic parameters for the disordered F-, O- and H-atoms, the following structural model was adopted at all six temperatures: a single O/F site including anisotropic displacement parameters (ADPs) was refined first. The site was then split into an oxygen (O5) and a fluorine (F) site with ADPs constrained to be equal. The distance between the O5 and F atoms was restrained to 0.15 Å ($\sigma = 0.01$) (SHELXL-97, command DFIX). This model accounts for the difference of 0.065 Å between the Mg–O and Mg–F distances arising from the difference in ionic radii (Shannon 1976), provided the O/F splitting occurs perpendicular to the Mg_3-plane of the Mg_3(OH/F) pyramid. This latter assumption is supported by experiment: ADPs obtained with a single atom show an elongated ellipsoid ('cigar') perpendicular to the Mg_3-plane. This observation is also in line with Pauli's principle of parsimony, which predicts that a group of atoms will adopt the most symmetric configuration in accordance with its atomic environment. The choice of the fixed O5···F distance is supported by a series of test refinements with different fixed O5···F distances. Values around 0.15 Å give the best results in terms of R-value, $\sigma[d(\text{O–H})]$, U_{eq}(O5) as well as ΔU along the interatomic vector (H–O5). Because the coherent neutron scattering length of F and O are too similar to distinguish between the two atom types (5.80 vs. 5.65), the site closer to the Mg ions was forced to be F in accordance with ionic radii. The resulting linear O–F unit was further constrained to lie parallel to the long axis of the observed nuclear density distribution ('cigar') by constraining the three Mg–O5 and Mg–F bonds, respectively, to have approximately equal lengths (SHELXL-97, command SADI, $\sigma = 0.01$). Occupation of the O5 site is required to equal that of the H site; the F-site occupation is constrained by the condition $p(\text{O5}) + p(\text{F}) = 1$. This condition ensures that each H-atom is associated with an oxygen rather than a fluorine atom (Friedrich et al. 2002). The occupations of the O5 and H sites are 0.43(1), the average value obtained from initial refinements of all data sets. The occupancy of Mg and Fe on the special position M1 was refined to values around 0.88/0.12 at all temperatures. This corresponds to $Mg_{4.87}Fe_{0.13}$ when normalized to eight oxygens, which is in slight disagreement with the Mg/Fe ratio as

Table 1 Details of neutron diffraction experiments, structure refinements and cell parameters of Tilly Foster chondrodite

	10 K	100 K	295 K	500 K	700 K	900 K
Measured in	Oak Ridge	Oak Ridge	Oak Ridge	ILL (D9)	ILL (D9)	ILL (D9)
No. of structure factors measured	1,567[a]	1,570	1,576	2,689	1,009	837
No. of structure factors rejected	151	151	151	144	0	65
No. of unique reflections.	1,335	1,338	1,343	1,001	1,009	722
R-Merge (%)	5.86	5.27	2.56	1.75	n/a	1.59
$\|F\|_{obs} > 4\sigma$	1,221	1,201	1,208	994	993	691
*R*1 (all data)[b] (%)	4.30	4.18	3.83	2.14	2.20	2.44
*R*1 ($>4\sigma$) (%)	3.75	3.53	3.26	2.10	2.11	2.23
*wR*2[c] (%)	9.71	8.95	8.39	4.52	4.27	4.80
Weighting coefficients *a*, *b*[c]	0.038 / 0.30	0.038 / 0.30	0.038 / 0.30	0.0076 / 0.462	0.0076 / 0.462	0.011 / 0.250
Extinction parameter *k*[d]	0.481	0.465	0.431	0.437	0.0003	0.321
Number of variables	94	94	94	94	94	94
a	4.7321(4)	4.7345(4)	4.7328(4)	4.7375(4)	4.7426(4)	4.7501(4)
b	10.2641(7)	10.2674(7)	10.2749(7)	10.2920(7)	10.3082(7)	10.3297(8)
c	7.8673(5)	7.8716(5)	7.8756(5)	7.8897(5)	7.9010(5)	7.9192(6)
α	109.052(3)	109.060(3)	109.065(3)	109.071(3)	109.072(3)	109.048(6)

Space group $P2_1/b$, *a* unique

[a]Refinement on *F* at 10 K, 100 K, and 293 K, on F^2 at 500 K, 700 K, 900 K

[b]$R1 = (\Sigma||F_{obs}| - |F_{calc}||)/(\Sigma|F_{obs}|)$

[c]The slightly increased *wR*2 of the LT data is probably due to shadowing of some reflections by the He-refrigerator (Friedrich et al. 2001) rather than to refinement against *F*. $wR2 = \{\Sigma[w(F^2_{obs} - F^2_{calc})^2]/\Sigma[w(F^2_{obs})^2]\}^{1/2}$, where $w = 1/[\sigma^2(F^2_{obs}) + (aP)^2 + bP]^{-1}$, where $P = [2F^2_{calc} + \mathrm{Max}(F^2_{obs}, 0)]/3$

[d]Extinction correction was done in the form of $F_c(\mathrm{corrected}) = Fc * [1 + 0.001\ k\ F_c^2\ \lambda^3/\sin(2\theta)]^{-1/4}$, *k* was refined

determined with the electron-microprobe ($Mg_{4.64}Fe_{0.28}$). We attribute this discrepancy to the presence of impurities (e.g. Mn and Ti) on the M-sites, which have not been accounted for by the refinement of the occupancies.

Results and discussion

Tables 1, 2, 3, 4, 5 report results in the temperature range between 10 and 900 K obtained from our high-temperature (HT) data and from the low-temperature data (LT) collected previously on the same crystal by Friedrich et al. (2001). Unit-cell parameters are given in Table 1, refined atomic coordinates in Table 2, and ADPs in Table 3. Selected bond lengths are given in Table 4. In Tables 5, 6 and 7 we report the results of our analysis of the thermal evolution of the atomic displacement parameters of O5 and H and of the resulting O–H bond length corrections.

Cell constants

At first glance, the HT unit cell parameters measured at ILL seem to be inconsistent with the RT/LT values from Oak Ridge (Fig. 1). This could be due to a systematic error, e.g. an incorrectly calibrated wavelength for one of the experiments. To test this, we compared the neutron data with a room-temperature data point collected with a sealed tube X-ray source (Friedrich et al. 2002), which is unambiguous with respect to wavelength. As can be seen in Fig. 1, this value fits smoothly into the trend of the ILL high-temperature data set. If we combine the ILL cell parameters with the X-ray room temperature values and extrapolate them to low-temperature using a second order polynomial (without a linear term to comply with the thermodynamic condition of zero slope at 0 K) we find predicted cell parameters at 10 K and 100 K, which are not significantly different from the observed neutron values reported by Friedrich et al. (2001). For this reason, the neutron unit cell parameters at 10 K and 100 K were used unchanged, while the neutron values at room temperature were replaced by the X-ray values. The reasons for the difference at room temperature are unclear, but cannot be traced to inaccuracies in wavelength calibration only, because the monoclinic angle, which depends only on distance ratios, is also affected (Fig. 1d).

Temperature dependence of Mg–O and Si–O bond lengths

The Mg–O bond lengths account for most of the thermal expansion; they increase steadily over the entire temperature range by about 0.015 Å, i.e. by 10 to 20 estimated standard deviations (Fig. 2). The average Si–O bond distance decreases slightly with increasing temperature (Fig. 3).

This is a well-known effect due to increased librational motion of the rigid SiO_4 group at higher temperatures. After applying the correction described by Downs (2000), the Si–O bond-lengths are essentially constant, as expected (Downs 1992).

O–H Bond lengths

Our O–H bond distances of ~0.94 Å are shorter than the values of 1.028(4)Å reported by Friedrich et al. (2001) at room temperature. This difference is due to

Table 2 Fractional coordinates and isotropic displacement parameters (Å^2) of Tilly Foster chondrodite between 10 and 900 K

	x	y	z	U_{iso}	x	y	z	U_{iso}	x	y	z	U_{iso}
	10 K				100 K				295 K			
M1	1/2	0	1/2	0.0052(3)	1/2	0	1/2	0.0058(3)	1/2	0	1/2	0.0083(3)
M2	0.0103(2)	0.17385(7)	0.3070(1)	0.0047(2)	0.0103(2)	0.17379(7)	0.30694(9)	0.0052(2)	0.0104(1)	0.17356(7)	0.30721(9)	0.0076(2)
M3	0.4924(2)	0.88650(8)	0.0795(1)	0.0057(2)	0.4924(2)	0.88657(7)	0.0795(1)	0.0062(2)	0.4921(1)	0.88630(7)	0.0791(1)	0.0085(2)
Si	0.0761(2)	0.14418(9)	0.7040(1)	0.0045(2)	0.0759(2)	0.14414(9)	0.7041(1)	0.0052(2)	0.0760(2)	0.14420(9)	0.7040(1)	0.0066(2)
O1	0.7789(2)	0.00114(7)	0.2939(1)	0.0058(2)	0.7789(2)	0.00113(7)	0.29396(9)	0.0064(2)	0.7792(1)	0.00095(7)	0.29416(9)	0.0084(2)
O2	0.7273(2)	0.24059(7)	0.1251(1)	0.0058(2)	0.7273(2)	0.24066(7)	0.12523(9)	0.0063(2)	0.7268(1)	0.24083(7)	0.12524(9)	0.0084(2)
O3	0.2241(2)	0.16888(7)	0.5285(1)	0.0058(2)	0.2241(1)	0.16890(7)	0.52841(9)	0.0065(2)	0.2238(1)	0.16898(7)	0.52863(9)	0.0086(2)
O4	0.2651(2)	0.85484(8)	0.2948(1)	0.0059(2)	0.2649(2)	0.85491(7)	0.29479(9)	0.0063(2)	0.2646(1)	0.85475(7)	0.29472(9)	0.0083(2)
O5	0.246(1)	0.0533(6)	0.0916(7)	0.0059(3)	0.246(1)	0.0533(6)	0.0918(7)	0.0065(3)	0.246(1)	0.0532(6)	0.0917(7)	0.0093(3)
F	0.2688(8)	0.0596(4)	0.1042(5)	0.0059(3)	0.2687(8)	0.0595(4)	0.1040(5)	0.0065(3)	0.2691(8)	0.0593(4)	0.1042(5)	0.0093(3)
H	0.0894(8)	0.0140(4)	0.0197(5)	0.0199(6)	0.0883(8)	0.0137(4)	0.0195(5)	0.0207(6)	0.0887(8)	0.0136(4)	0.0194(5)	0.0254(6)
	500 K				700 K				900 K			
M1	1/2	0	1/2	0.0081(2)	1/2	0	1/2	0.0112(2)	1/2	0	1/2	0.0144(3)
M2	0.0104(1)	0.17338(5)	0.30720(7)	0.00747(9)	0.0106(1)	0.17317(4)	0.30750(6)	0.01029(8)	0.0106(2)	0.17278(7)	0.3077(1)	0.0128(2)
M3	0.4917(1)	0.88608(5)	0.07902(7)	0.00810(9)	0.4913(1)	0.88585(5)	0.07874(6)	0.01097(8)	0.4910(2)	0.88556(8)	0.0785(1)	0.0137(2)
Si	0.0764(1)	0.14428(6)	0.70407(8)	0.0053(1)	0.0764(1)	0.14429(5)	0.70404(7)	0.00703(8)	0.0766(2)	0.14445(9)	0.7039(1)	0.0087(2)
O1	0.7794(1)	0.00060(4)	0.29406(6)	0.00778(8)	0.77955(9)	0.00036(4)	0.29422(6)	0.01037(7)	0.7800(1)	0.00004(7)	0.29439(9)	0.0128(1)
O2	0.7267(1)	0.24097(5)	0.12552(6)	0.00803(8)	0.72627(9)	0.24116(4)	0.12571(5)	0.01072(7)	0.7259(1)	0.24156(6)	0.12591(9)	0.0135(1)
O3	0.2235(1)	0.16901(5)	0.52906(6)	0.00783(8)	0.22333(9)	0.16910(4)	0.52937(5)	0.01046(7)	0.2233(1)	0.16916(7)	0.52968(9)	0.0130(1)
O4	0.26390(9)	0.85468(5)	0.29459(6)	0.00763(8)	0.26330(8)	0.85451(4)	0.29455(5)	0.01019(7)	0.2626(1)	0.85449(7)	0.29471(9)	0.0128(1)
O5	0.247(1)	0.0532(4)	0.0922(5)	0.0100(3)	0.247(7)	0.0531(6)	0.0923(7)	0.0135(3)	0.247(1)	0.0529(6)	0.0921(7)	0.0172(3)
F	0.2686(8)	0.0592(4)	0.1038(5)	0.0100(3)	0.2685(8)	0.0589(4)	0.1038(5)	0.0135(3)	0.2693(9)	0.0589(5)	0.1043(6)	0.0172(3)
H	0.0899(6)	0.0139(3)	0.0197(4)	0.0272(5)	0.0907(6)	0.0141(3)	0.0201(4)	0.0344(5)	0.0924(9)	0.0146(5)	0.0215(6)	0.0410(9)

Occupancy of H and O5 was fixed at 0.43 for all final refinements at all temperatures. Occupancy of *F* was fixed to 0.57. Occupancy of Mg on the M1 position was refined to values around 0.88 at all temperatures. Occupancy of Fe on the same site was constrained to 0.12. U_{ij}(*F*) was constrained to equal U_{ij}(O5). U_{iso} is defined according to Hamilton (1959)

Table 3 Anisotropic displacement parameters U_{ij}[a] (in Å^2) of Tilly Foster chondrodite between 10 and 900 K

	U_{11}	U_{22}	U_{33}	U_{12}	U_{13}	U_{23}	U_{11}	U_{22}	U_{33}	U_{12}	U_{13}	U_{23}
	10 K						100 K					
M1	0.0038(5)	0.0057(4)	0.0051(5)	0.000(3)	−0.0001(3)	0.0003(3)	0.0055(5)	0.0055(4)	0.0054(4)	0.0003(3)	0.0000(3)	0.0005(3)
M2	0.0034(3)	0.0046(3)	0.0056(3)	0.0002(2)	0.0003(2)	0.0009(2)	0.0047(3)	0.0050(3)	0.0055(3)	0.0000(2)	0.0004(2)	0.0011(2)
M3	0.0047(3)	0.0057(3)	0.0061(3)	−0.0003(2)	−0.0003(2)	0.0012(2)	0.0058(3)	0.0062(3)	0.0063(3)	0.0001(2)	−0.0003(2)	0.0016(2)
Si	0.0031(4)	0.0050(4)	0.0050(4)	−0.0001(3)	0.0002(3)	0.0009(3)	0.0039(4)	0.0055(3)	0.0054(4)	−0.0001(3)	−0.0003(3)	0.0010(3)
O1	0.0051(3)	0.0056(3)	0.0064(3)	0.0001(2)	0.0001(2)	0.0014(2)	0.0062(3)	0.0058(3)	0.0068(3)	0.0000(2)	0.0001(2)	0.0017(2)
O2	0.0043(3)	0.0058(3)	0.0061(3)	0.0003(2)	0.0006(2)	0.0004(2)	0.0057(3)	0.0058(3)	0.0062(3)	−0.0002(2)	0.0004(2)	0.0002(2)
O3	0.0046(3)	0.0068(3)	0.0058(3)	−0.0002(2)	0.0002(2)	0.0017(2)	0.0058(3)	0.0071(3)	0.0065(3)	−0.0001(2)	0.0002(2)	0.0022(2)
O4	0.0040(3)	0.0065(3)	0.0065(3)	0.0003(2)	0.0002(2)	0.0013(2)	0.0049(3)	0.0068(3)	0.0065(3)	−0.0001(2)	−0.0002(2)	0.0013(2)
O5[b]	0.0048(6)	0.0058(4)	0.0060(6)	−0.0008(4)	−0.0003(5)	0.0004(4)	0.0057(6)	0.0063(4)	0.0063(5)	−0.0007(4)	−0.0002(4)	0.0006(4)
H	0.012(1)	0.023(1)	0.021(1)	−0.003(1)	−0.004(1)	0.001(1)	0.012(1)	0.025(1)	0.021(1)	−0.003(1)	−0.005(1)	0.002(1)
	295 K						500 K					
M1	0.0068(4)	0.0085(4)	0.0084(4)	0.0006(3)	0.0005(3)	0.0012(3)	0.0064(3)	0.0086(3)	0.0078(3)	0.0010(2)	0.0013(2)	0.0006(2)
M2	0.0067(3)	0.0071(3)	0.0090(3)	−0.0001(2)	−0.0001(2)	0.0025(2)	0.0074(2)	0.0069(2)	0.0085(2)	0.0003(1)	−0.0001(1)	0.0031(1)
M3	0.0082(3)	0.0087(3)	0.0085(3)	0.0001(2)	−0.0003(2)	0.0026(2)	0.0083(2)	0.0085(2)	0.0078(2)	−0.0001(1)	−0.0007(1)	0.0031(1)
Si	0.0038(3)	0.0076(3)	0.0080(3)	0.0001(2)	0.0003(2)	0.0022(2)	0.0037(2)	0.0062(3)	0.0060(2)	−0.0001(2)	−0.0001(2)	0.0019(2)
O1	0.0076(3)	0.0076(3)	0.0098(3)	−0.0002(2)	0.0003(2)	0.0027(2)	0.0074(2)	0.0064(2)	0.0101(2)	0.0002(1)	0.0003(1)	0.0035(1)
O2	0.0070(3)	0.0081(3)	0.0088(3)	−0.0000(2)	0.0006(2)	0.0008(2)	0.0072(2)	0.0075(2)	0.0075(2)	−0.0002(1)	0.0006(1)	−0.0002(1)
O3	0.0072(3)	0.0101(3)	0.0088(3)	−0.0003(2)	0.0002(2)	0.0037(2)	0.0070(2)	0.0103(2)	0.0072(2)	−0.0003(1)	0.0001(1)	0.0043(1)
O4	0.0056(3)	0.0092(3)	0.0095(3)	−0.0000(2)	0.0001(2)	0.0025(2)	0.0043(2)	0.0094(2)	0.0091(2)	−0.0001(1)	0.0001(1)	0.0028(1)
O5[b]	0.0078(6)	0.0090(4)	0.0103(5)	−0.0000(4)	0.0006(4)	0.0022(4)	0.0097(5)	0.0094(3)	0.0104(5)	0.0005(4)	0.0017(4)	0.0027(3)
H	0.015(1)	0.030(2)	0.027(1)	−0.004 (1)	−0.007(1)	0.003(1)	0.018(1)	0.030(1)	0.028(1)	−0.0038(8)	−0.0057(8)	0.0025(9)
	700 K						900 K					
M1	0.0089(2)	0.0122(2)	0.0105(2)	0.0017(2)	0.0019(2)	0.0010(2)	0.0105(4)	0.0161(4)	0.0141(4)	0.0020(3)	0.0023(3)	0.0016(3)
M2	0.0101(2)	0.0096(2)	0.0117(2)	0.0005(1)	−0.0002(1)	0.0043(1)	0.0122(3)	0.0127(3)	0.0144(3)	0.0007(2)	−0.0004(2)	0.0055(2)
M3	0.0111(2)	0.0114(2)	0.0107(2)	−0.0001(1)	−0.0012(1)	0.0040(1)	0.0130(3)	0.0151(3)	0.0134(3)	−0.0003(2)	−0.0015(2)	0.0052(2)
Si	0.0047(2)	0.0082(2)	0.0079(2)	−0.0002(1)	−0.0000(1)	0.0022(1)	0.0050(3)	0.0104(3)	0.0105(3)	−0.0002(2)	−0.0002(3)	0.0031(3)
O1	0.0097(1)	0.0085(1)	0.0137(1)	0.0002(1)	0.0004(1)	0.0047(1)	0.0115(3)	0.0109(2)	0.0169(3)	0.0006(2)	0.0007(2)	0.0057(3)
O2	0.0094(1)	0.0102(1)	0.0100(1)	−0.0003(1)	0.0008(1)	−0.0001(1)	0.0111(3)	0.0133(3)	0.0127(3)	−0.0004(2)	0.0010(2)	−0.0006(2)
O3	0.0089(1)	0.0142(2)	0.0097(1)	−0.0003(1)	0.0003(1)	0.0058(1)	0.0106(3)	0.0183(3)	0.0118(3)	−0.0005(2)	0.0005(2)	0.0074(2)
O4	0.0054(1)	0.0128(2)	0.0122(1)	−0.0001(1)	0.0002(1)	0.0039(1)	0.0059(2)	0.0170(3)	0.0154(3)	−0.0001(2)	0.0004(2)	0.0050(2)
O5[b]	0.0129(5)	0.0130(3)	0.0144(4)	0.0010(3)	0.0026(4)	0.0041(3)	0.0155(6)	0.0172(4)	0.0188(3)	0.0010(4)	0.0031(5)	0.0056(4)
H	0.023(1)	0.039(1)	0.035(1)	−0.0055(9)	−0.0075(9)	0.004(1)	0.029(2)	0.044(2)	0.042(2)	−0.006(2)	−0.007(2)	0.004(2)

[a] U_{ij} are defined as $U_{ij} = \sum_{k}^{3} \sigma_k^2 \cos\left(a_j^* < c_k\right) \cos\left(a_j^* < c_k\right)$, where σ_k are the mean-square displacement amplitudes with respect to a Cartesian basis of principal vectors c_k of the tensor U_{ij} and a^*_1, a^*_2, a^*_3 refer to the reciprocal basis vectors a^*, b^*, c^*, respectively

[b] $U_{ij}(F)$ were constrained to equal U_{ij}(O5)

Table 4 Selected interatomic distances (in Å) of Tilly Foster chondrodite between 10 and 900 K

	10 K	100 K	295 K	500 K	700 K	900 K
M1–O1 (2x)	2.0937(7)	2.0945(7)	2.0940(7)	2.0972(5)	2.0989(4)	2.1024(7)
M1–O3 (2x)	2.1227(7)	2.1239(7)	2.1255(7)	2.1292(5)	2.1330(4)	2.1372(7)
M1–O4 (2x)	2.1192(7)	2.1203(7)	2.1228(7)	2.1285(5)	2.1338(4)	2.1399(7)
Average	2.1119	2.1129	2.1141	2.1183	2.1219	2.1265
M2–O1	2.0574(9)	2.0578(9)	2.0576(9)	2.0616(7)	2.0647(6)	2.067(1)
M2–O2	2.225(1)	2.226(1)	2.2314(9)	2.2353(7)	2.2429(6)	2.253(1)
M2–O3	2.030(1)	2.031(1)	2.0292(9)	2.0339(7)	2.0348(6)	2.038(1)
M2–O3	2.180(1)	2.181(1)	2.1821(9)	2.1859(7)	2.1890(6)	2.194(1)
M2–O4	2.169(1)	2.172(1)	2.1748(9)	2.1809(6)	2.1862(6)	2.196(1)
M2–O5' [a]	2.068(5)	2.068(5)	2.070(5)	2.072(5)	2.075(5)	2.081(5)
Average	2.1216	2.1226	2.1242	2.1283	2.1321	2.1382
M3–O1	2.184(1)	2.186(1)	2.1906(9)	2.1951(7)	2.2016(6)	2.210(1)
M3–O2	2.001(1)	2.002(1)	1.9994(9)	2.0015(7)	2.0016(6)	2.005(1)
M3–O2	2.117(1)	2.118(1)	2.119(1)	2.1219(7)	2.1256(6)	2.128(1)
M3–O4	2.120(1)	2.121(1)	2.123(1)	2.1263(7)	2.1310(6)	2.138(1)
M3–O5	2.048(5)	2.048(5)	2.048(5)	2.049(5)	2.051(5)	2.055(5)
M3–O5' [a]	2.067(5)	2.067(5)	2.069(5)	2.074(5)	2.078(5)	2.083(6)
Average	2.0900	2.0903	2.0915	2.0946	2.0981	2.1032
Si–O1	1.647(1)	1.647(1)	1.646(1)	1.6446(7)	1.6443(7)	1.645(1)
Si–O2	1.637(1)	1.637(1)	1.636(1)	1.6346(7)	1.6342(6)	1.634(1)
Si–O3	1.641(1)	1.643(1)	1.640(1)	1.6391(7)	1.6389(6)	1.639(1)
Si–O4	1.615(1)	1.614(1)	1.612(1)	1.6122(7)	1.6112(7)	1.611(1)
Average	1.635	1.6353	1.6354	1.6326	1.6322	1.6323

[a] O5' is related to O5 by a center of symmetry

Table 5 Atomic and correlation displacement parameters of O–H group in a local coordinate system (observed and calculated)[a] [b]

	10 K	100 K	295 K	500 K	700 K	900 K
U^*_{11}(O5)[a] (Å^2)	0.0043(5)	0.0052(5)	0.0088(5)	0.0112(5)	0.0156(5)	0.0192(5)
U^*_{22}(O5) (Å^2)	0.0058(5)	0.0061(5)	0.0087(5)	0.0085(5)	0.0113(5)	0.0146(5)
U^*_{33}(O5) (Å^2)	0.0076(5)	0.0081(5)	0.0103(5)	0.0101(5)	0.0137(5)	0.0178(5)
$\alpha_{obs} = [U^*_{22}(O5) + U^*_{33}(O5)]/2$ (Å^2)	0.0067(5)	0.0071(5)	0.0095(5)	0.0093(5)	0.0125(5)	0.0162(5)
α_{calc}, Bürgi–Capelli model (Å^2)	0.0073	0.0073	0.0087	0.0107	0.0130	0.0152
U^*_{11}(H) (Å^2)	0.010(1)	0.010(1)	0.012(1)	0.015(1)	0.018(1)	0.024(2)
U^*_{22}(H) (Å^2)	0.020(1)	0.023(1)	0.028(1)	0.029(1)	0.037(1)	0.044(2)
U^*_{33} (H) (Å^2)	0.029(1)	0.030(1)	0.036(1)	0.038(1)	0.048(1)	0.055(2)
$\beta_{obs} = [U^*_{22}(H) + U^*_{33}(H)]/2$ (Å^2)	0.025(1)	0.026(1)	0.032(1)	0.034(1)	0.043(1)	0.049(1)
β_{calc}, Bürgi–Capelli model (Å^2)	0.0261	0.0262	0.0289	0.0347	0.0421	0.0502
γ_{calc}, lower limit (Å^2)	0.0129	0.0137	0.0175	0.0177	0.0230	0.0283
γ_{calc}, riding model (Å^2)	0.0067	0.0071	0.0095	0.0093	0.0125	0.0162
γ_{calc}, Bürgi–Capelli model (Å^2)	0.0023	0.0023	0.0040	0.0065	0.0090	0.0116
γ_{calc}, independent motion (Å^2)	0	0	0	0	0	0
γ_{calc}, upper limit (Å^2)	−0.0129	−0.0137	−0.0175	−0.0177	−0.0230	−0.0283
ΔU(O–H) (Å^2)	0.0056(15)	0.0043(15)	0.0028(15)	0.0034(15)	0.0025(15)	0.0048(15)

[a] U^*_{ij} corresponds to U_{ij} transformed into a local, orthogonal, right-handed coordinate system with U^*_{11} parallel to the O–H vector according to the transformation matrix [0.79 0.25 0.49 / 0.60 −0.09 −0.77 / −0.14 −1.03 −0.5]
[b] α, β and γ as defined by Johnson (1970) and described in text

differences in refinement strategies: we use a split-atom description, whereas Friedrich et al. (2001) modeled the O–F dumbbell with a single atom. Our O–H bonds are also shorter than the typical values for O–H bonds of ~0.97(1) Å given by Ceccarelli et al. (1981). This difference is likely to be due to riding motion of the light H-atom on the relatively heavy oxygen atom. Such an interpretation is further supported by the decrease of the O–H distance with increasing temperatures, an effect that resembles the behaviour of the Si–O bonds. These effects need to be corrected for if we want to relate the temperature dependence of the O–H bond distances with O–H stretching frequencies. As shown by Johnson (1970), the appropriate distance correction for a diatomic structural unit requires knowledge of the perpendicular mean-square amplitudes α of O5, β of H and the mean square correlation amplitude γ of the two atoms. Together they form the mean square displacement matrix $\sum = \begin{bmatrix} \alpha & \gamma \\ \gamma & \beta \end{bmatrix}$. The corrected bond length $d(\text{O–H})_{cor}$ is then calculated from the observed value $d(\text{O–H})_{obs}$ as:

Table 6 Frequencies and eigenvectors of parallel and perpendicular O–H vibrations with temperature independent corrections ε from the Bürgi-Capelli model

	Frequencies (cm^{-1})	Eigenvectors	T-independent $\varepsilon_O = \varepsilon_H$ ($Å^2$)
Perpendicular to O–H bond	888, 338	$\begin{pmatrix} 0.9511 \\ -0.3087 \end{pmatrix}$ $\begin{pmatrix} 0.3087 \\ 0.9511 \end{pmatrix}$	0.0011
Parallel to O–H bond	3514, 263	$\begin{pmatrix} 0.9715 \\ -0.2370 \end{pmatrix}$ $\begin{pmatrix} 0.2370 \\ 0.9715 \end{pmatrix}$	0.0043

Table 7 Observed and corrected O–H distances as a function of temperature

	10 K	100 K	295 K	500 K	700 K	900 K
O5–H (uncorrected) (Å)	0.939(7)	0.947(7)	0.945(7)	0.945(6)	0.942(6)	0.929(8)
O5–H (corrected) (Å)	0.970(7)	0.977(7)	0.976(7)	0.980(6)	0.981(6)	0.975(8)
H···F (uncorrected) (Å)	1.978(7)	1.972(7)	1.975(7)	1.980(6)	1.986(6)	2.006(8)
H···F (corrected) (Å)[a]	1.943(7)	1.938(7)	1.940(7)	1.942(7)	1.9428	1.9574

[a]The corrected H···F hydrogen bond is calculated geometrically using the corrected O–H bond, the O5···F distance and the observed O–H···F angle

$$d(\text{O--H})_{\text{cor}} = d(\text{O--H})_{\text{obs}} + \frac{(\alpha + \beta - 2\gamma)}{[2d(\text{O--H})_{\text{obs}}]} \quad (1)$$

From a diffraction experiment at a single temperature, only the diagonal elements α and β can be obtained. The off-diagonal term γ, which depends on the relative movements of different atoms, is indeterminate. This lack of information on γ is sometimes referred to as the second phase problem in crystallography. Since the eigenvalues of Σ cannot be negative, the condition $|\gamma| < (\alpha\beta)^{1/2}$ holds and places constraints on the limiting values of γ and, thus, on the range of possible bond length corrections (Johnson 1970). The upper and lower limits of the corrections are $\gamma = -(\alpha\beta)^{1/2}$ and $\gamma = (\alpha\beta)^{1/2}$, respectively. The so-called riding model corresponds to $\gamma = \alpha$ (Busing and Levy 1964). The model of independent motion implies $\gamma = 0$ (Fig. 4).

Bürgi and Capelli (2000) have recently shown how to determine the off-diagonal term γ from the temperature dependence of the atomic mean square displacements α and β, and, thus, how to correct the O–H bond distance without assuming one of the above models. Their approach is based on the fact that the mean-square displacement matrix Σ depends on the atomic masses, the atomic displacements and the mean-square amplitudes of the normal modes, in matrix notation: $\Sigma = \mathbf{m^{-1/2}e\delta e^T m^{-1/2}}$, where $\mathbf{m}$ is a diagonal atomic mass matrix, $\mathbf{e}$ is the orthonormal matrix of vibrational eigenvectors ($\mathbf{e^T}$ its transpose) and $\boldsymbol{\delta}$ is a diagonal matrix whose elements are the mean square amplitudes of the normal modes. Using the Bose–Einstein distribution law, the temperature dependence of Σ follows from the temperature dependence of the elements of $\boldsymbol{\delta}$:

$$\delta_i = \left(\frac{\hbar}{2\omega_i}\right) \coth\left(\frac{\hbar\omega_i}{2k_B T}\right), \quad (2)$$

where ω_i is a normal mode frequency, k_B the Boltzman constant and $\hbar$ the $1/2\pi$-weighted Planck constant. At high temperatures δ_i equals $k_B T/\omega_i^2$, whereas at low temperatures δ_i is $\hbar/2\omega_i$, independent of T and, thus, with a finite value at 0 K. It is this different behaviour at low and high temperatures, which allows retrieving the off-diagonal elements of Σ. A more detailed description of this approach is given in Bürgi and Capelli (2000).

In our case, the off-diagonal terms may be calculated after determining the components of the orthonormal 2×2 matrix $\mathbf{e}$ (one variable) and the two frequencies of the two normal modes (two variables) by a least squares procedure from the 12 observed displacement amplitudes of O5 and H, respectively. The latter were taken to be the average of the two mean-square displacements perpendicular to the O–H bond (Table 5).

In order to account for temperature-independent contributions to the ADPs arising from residual disorder at the O5/F site or from systematic errors either in the diffraction data or the structural model, we introduced an additional, temperature independent variable ε, which is added to the temperature dependent part to give $\Sigma = \mathbf{m^{-1/2}e\delta e^T m^{-1/2}} + \varepsilon$. It takes the form of a diagonal 2×2 matrix with $\varepsilon_O = \varepsilon_H$. The function to be minimized is the sum of the squares of the unweighted differences between calculated and observed diagonal elements of the mean-square displacement matrix. The non-linear least-squares refinement was done using the function 'Solver' within Microsoft-Excel. Observed and calculated values of α, β and γ are reported in Table 5. Frequencies and eigenvectors of parallel and perpendicular O–H vibrations with temperature independent corrections, as well as O–H bond-distances corrected using Eq. 1, and α, β and γ according to Johnson (1970) are given in Tables 6 and 7.

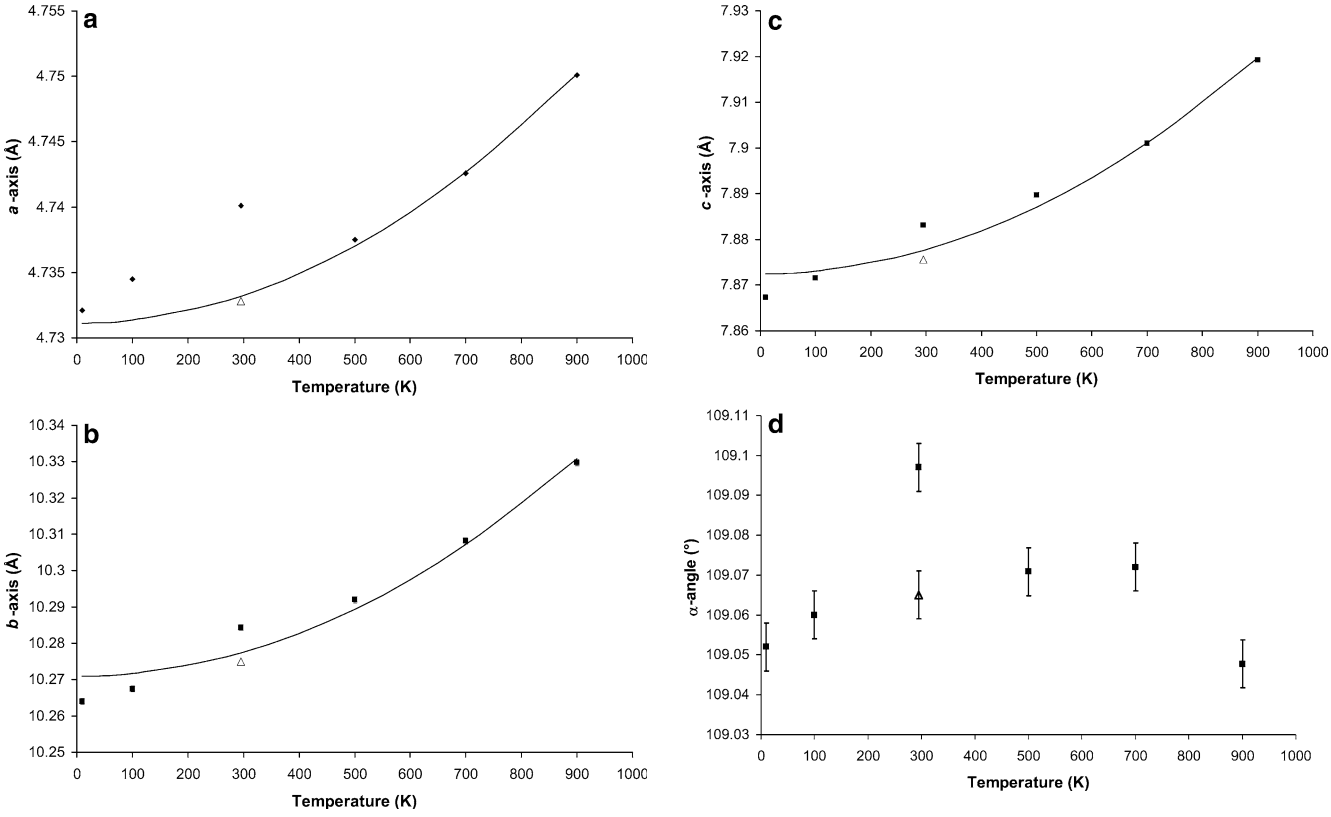

Fig. 1 Cell parameters of Tilly Foster chondrodite between 10 and 900 K. **a** *a*-axis, the *solid line* represents a second-order polynomial fit $a = 4.731 + 2.36\times10^{-8}\cdot T^2$ **b** *b*-axis, the *solid line* represents a second-order polynomial fit $b = 10.271 + 7.40\times10^{-8}\cdot T^2$ **c** *c*-axis, the *solid line* represents a second-order polynomial fit $c = 7.873 + 5.83\times10^{-8}\cdot T^2$ **d** α-angle. Polynomial fits are calculated using the X-ray data at 300 K and the neutron data at higher temperatures. Experimental uncertainties of the unit cell lengths are smaller than the symbol size. *Open triangles* denote the room-temperature X-ray values from Friedrich et al. (2002). Estimated standard deviations (1σ) are smaller than symbols

Three observations attest to the reliability of our procedure

1. Observed and calculated U_{ij} values parallel and perpendicular to the O–H bond plotted against temperature for both the O and H atom agree across the entire temperature range from 10 to 900 K (Table 5, Fig. 5).
2. Good agreement between calculated and observed vibrational frequencies: Mernagh et al. (1999) observed a number of Raman bands in the range 500–960 cm^{-1}. They assigned OH-bending modes to spectral features below 750 cm^{-1}, which suggests that our refined frequency (888 cm^{-1}, Tables 6, 7) is somewhat too high. However, in view of the large number of absorption bands in the observed range and the difficulty in assigning them to specific modes, we do not weigh this difference heavily. An analogous analysis along the O–H direction resulted in a frequency of ~3,500 cm^{-1} for the O–H stretching motion (Tables 6 and 7), in agreement with both the observed value (Mernagh et al. 1999) and the range of known O–H stretching frequencies in minerals (Libowitzky 1999). The two modes describing in-phase motion of the two atoms are substantially lower in energy and of similar magnitude, 338 and 263 cm^{-1}, as expected for motion of mainly translational character. These findings are encouraging, since they suggest that the off-diagonal γ-terms given in Table 5 and used for correcting the O–H bond-lengths are also reasonable.
3. The temperature-independent correction term ε_O (ε_H) is rather small, as expected (Tables 6 and 7). In fact the contribution to the perpendicular motion (0.0011 $Å^2$) is in the range of the experimental uncertainties for α and β. The respective value for the motion parallel to the O–H bond is somewhat larger (0.0043 $Å^2$). We attribute this to remaining imperfections in our model for the O5/F positional disorder, which will be reflected, at least partially, in the ADPs. While we assumed and constrained the O5/F splitting to occur perpendicular to the Mg_3-plane (see above), the real configuration may well be slightly tilted relative to this axis with possibly even a static or dynamic disorder. Our data, however, do not allow us to resolve such a subtle tilt.

Figure 4 shows that the magnitudes of the minimal and maximal corrections are unreasonable, whereas the values for the riding model on one hand and for the model of independent motion on the other nicely

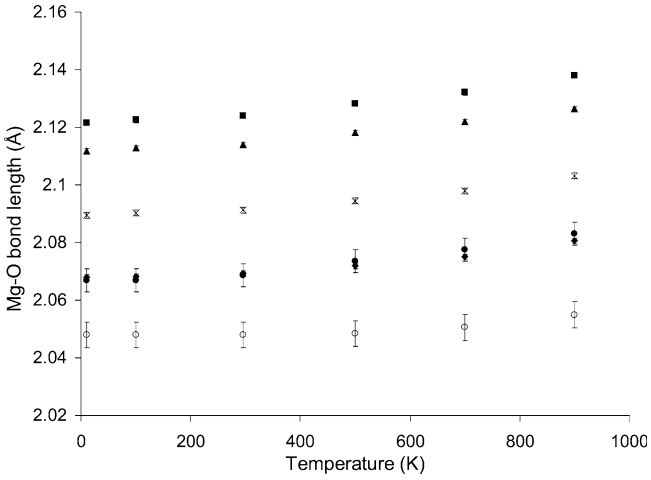

Fig. 2 Mg–O bond lengths of Tilly Foster chondrodite between 10 and 900 K. *filled diamond* Mg2–O5; *filled square* Mg2 average; *filled triangle* Mg1 average; *open circle* Mg3–O5; *star* Mg3 average; *filled circle* Mg3–O5'. O5' is related to O5 by a center of symmetry. *Error bars* indicate one estimated standard deviation

bracket the O–H distance derived from the temperature dependence of the ADPs. The deviations from the mean distance after correction according to the Bürgi–Capelli model are ~0.005 Å, well within the experimental uncertainty indicated by the scatter of the O–H bond lengths and the corresponding error bars (1σ). The mean distance also agrees with the reference value given by Ceccarelli et al. (1981).

Conclusions from a comparison of structural results with spectroscopic data

Bond distances may be related to stretching frequencies with the help of bond order-bond length-stretching frequency relationships. From the observed decrease in the

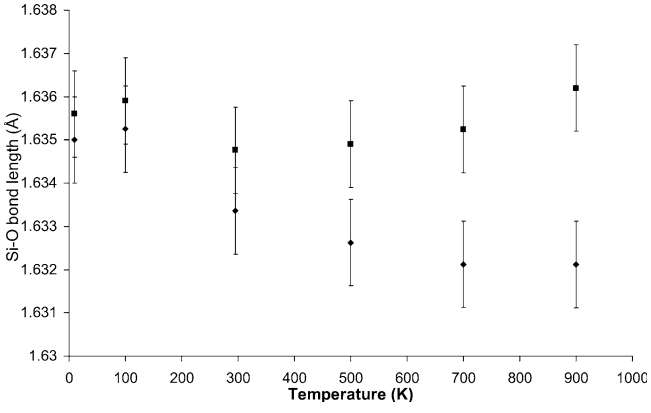

Fig. 3 Average Si–O bond length of Tilly Foster chondrodite between 10 and 900 K. Note the apparent shortening of the Si–O distance at high temperature due to an increased librational motion. If corrected for this effect, the Si–O bond distances are almost independent of temperature. *filled diamond* uncorrected Si–O bond length; *filled square* corrected for libration (Downs et al. 2000). Error bars indicate one estimated standard deviation

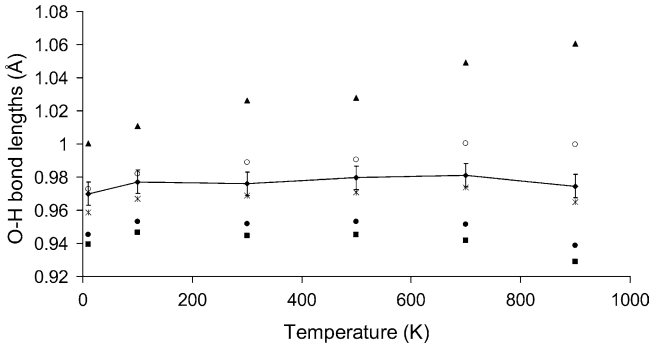

Fig. 4 Effect of various models of motion on the O–H distance correction for Tilly Foster chondrodite between 10 and 900 K. *filled triangle* upper limit; *open circle* independent motion; *filled diamond* according to Bürgi and Capelli (2000); *star* riding model; *filled circle* lower limit; *filled square* uncorrected. See text for details. *Error bars* indicate one estimated standard deviation

O–H stretching frequencies with increasing temperature, a minute OH-bond lengthening Δr of ~ 0.003 Å is estimated, a change that is well within the uncertainty of our results from neutron diffraction [$\Delta r \sim 0.5 \ln(\omega_{LT}/\omega_{HT})$, Bürgi and Dunitz (1987); $\omega_{10\ K} = 3{,}575\ cm^{-1}$ and $\omega_{900\ K} = 3{,}555\ cm^{-1}$, Mernagh et al. (1999)].

In contrast, the O5···F distance increases by ~0.02 Å (Fig. 6), a change similar to that of the Mg–O distances, but exceeding changes in the O–H distance by an order of magnitude (Fig. 7). This finding contradicts the strengthening (i.e. shortening) of the H···F hydrogen-bond deduced indirectly from a decrease in O–H stretching frequency, suggesting that one has to be careful when extrapolating from observed O–H frequencies to the strength, and especially the length of hydrogen bonds.

In summary, the O–H bond length in Tilly Foster chondrodite seems to be essentially independent of temperature within the accuracy attainable from a diffraction experiment on this partially disordered material, although a minute trend towards larger distances with increasing temperature cannot be excluded. Thus our findings do not contradict the weakening of the covalent O–H bonds indicated by spectroscopic measurements. The observed high stability of chondrodite in general, and the increased stability of F-bearing chondrodite in particular, is very unlikely to be due to a temperature induced strengthening of the H···F hydrogen bond as suspected on the basis of spectroscopic studies. From our findings, combined with results of Stalder and Ulmer (2001), Friedrich et al. (2001, 2002), and Lager et al. (2001), we conclude that the stability of chondrodites is determined primarily by the propensity of the Mg-silicate framework to disintegrate rather than to dehydrate. Nevertheless, it is also affected to some extent by the relative composition of the fluid component (OH/F ratio), since a OH/F ratio greater than one necessitates the occupation of a second hydrogen site. The additional hydrogen atom forms two hydrogen bonds, one of 2.149(4) Å to O1 and a weaker one of 2.251(3) Å to O2.

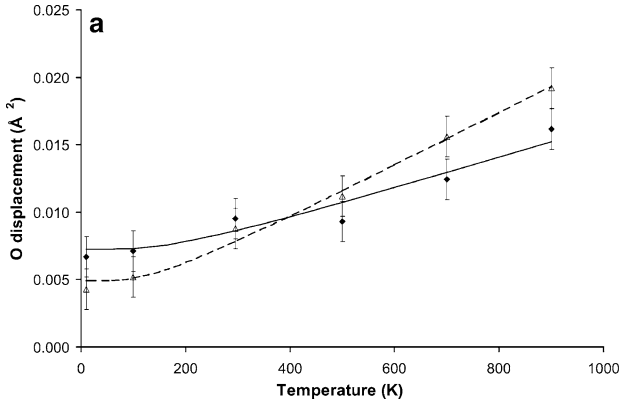

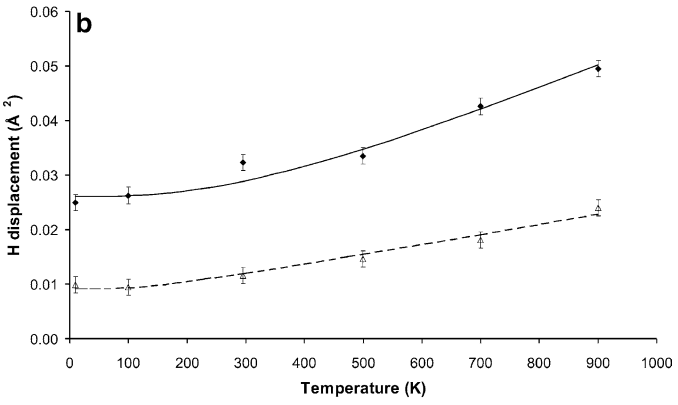

Fig. 5 Evolution of displacement parameters of U^*(O5) (**a**) and U^*(H) (**b**) with temperature. The *solid and dashed lines* give the results of the Bürgi–Capelli model for the vibrations perpendicular (*filled diamond*) and parallel *open triangle* to the O–H vector, respectively. *Error bars* indicate one estimated standard deviation. See text for details

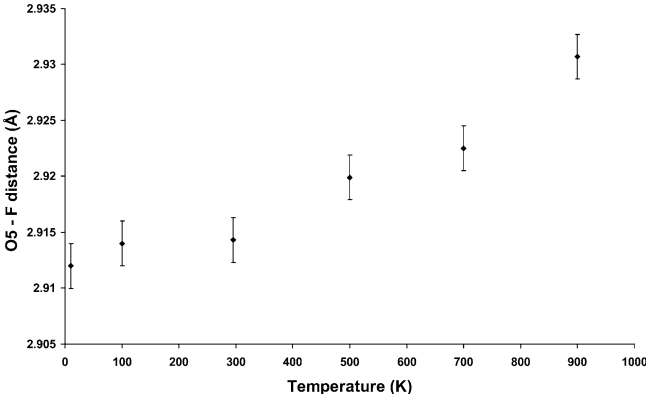

Fig. 6 O5–F distances in Tilly–Foster chondrodite between 10 and 900 K. The significant increase indicates a temperature-induced opening of the chondrodite framework around the H-atom. *Error bars* indicate one estimated standard deviation

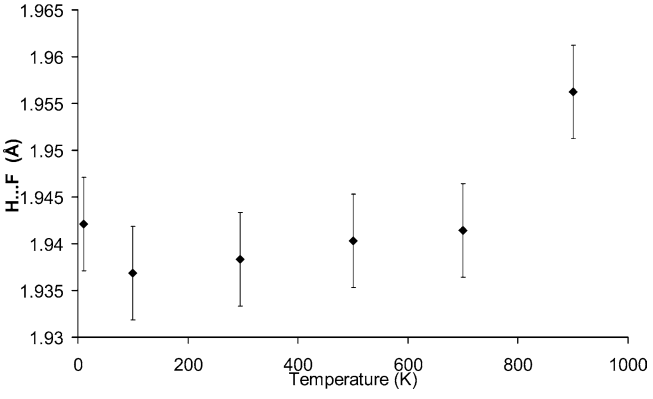

Fig. 7 H···F hydrogen bonds of Tilly Foster chondrodite between 10 and 900 K. *Error bars* indicate one estimated standard deviation

This withdraws electrons from the acceptor oxygen atoms and destabilizes the Mg-silicate framework somewhat. In pure OH-chondrodite, the magnesium–oxygen and silicon–oxygen bonds involving O1 (Lager et al. 2001) is lengthened relative to our F-bearing-chondrodite by ~0.013(2) Å on average, a difference of 6–7σ. The lengthening is insignificant for O2, which forms the second, weaker hydrogen bond (~0.000(2) Å, small for O3 (~0.005(2) Å) and O5 (~0.007(2) Å), and again relatively large for O4 (0.012(2) Å). In view of the consistently longer distances in OH-chondrodite, it thus seems reasonable to attribute the slightly lower stability relative to F-bearing chondrodite to a difference in hydrogen bonding and an associated difference in the strength of the framework bonds.

Disclaimer

Acknowledgments The authors acknowledge the support of the ILL staff ensuring a successful experiment. We thank Dr. Alexandra Friedrich for access to her low temperature data collected at Oak Ridge. GL is supported by NSF grant No. EAR-0073734. MK's work was supported by COMPRES, the Consortium for Materials

Properties Research in Earth Sciences under NSF Cooperative Agreement EAR 01-35554. HBB acknowledges support by the 'Schweizerischer Nationalfonds'.

References

Brown ID (2002) The chemical bond in inorganic chemistry. The bond valence model. IUCr Monographs on Crystallography, 12. Oxford University Press, Oxford

Bürgi HB, Capelli SC (2000) Dynamics of molecules in crystals from multi-temperature anisotropic displacement parameters. I. Theory. Acta Crystallogr A56:403–412

Bürgi HB, Dunitz JD (1987) Fractional bonds: relations among their lengths, strengths and stretching force constants. J Am Chem Soc 109:2924–2926

Busing WR, Levy HA (1964) The effect of thermal motion on the estimation of bond lengths from diffraction measurements. Acta Crystallogr 17:142–146

Ceccarelli C, Jeffrey GA, Taylor R (1981) A survey of O-H...O hydrogen bond geometries determined by neutron diffraction. J Mol Struct 70:255–271

Coppens P, Leiserowitz L, Rabinovich D (1965) Calculation of absorption corrections for camera and diffractometer data. Acta Crystallogr 18:1035–1038

Downs RT, Gibbs GV, Bartelmehs KL, Boisen MB Jr (1992) Variations of bond lengths and volumes of silicate tetrahedra with temperature. Am Mineral 77:751–757

Downs RT (2000) Analysis of harmonic displacement factors. Reviews in Mineralogy and Geochemistry, 41, High-temperature and high-pressure crystal chemistry. In: Hazen RM, Downs RT (eds) Mineralogical Society of America, Washington DC

Downs RT, Hall-Wallace M (2003) The American mineralogist crystal structure database. Am Mineral 88:247–250

Farrugia LJ (1999) WinGX suite for small-molecule single-crystal crystallography. J Appl Crystallogr 32:837–838

Friedrich A, Lager GA, Kunz M, Chakoumakos BC, Smyth JR, Schultz AJ (2001) Temperature-dependent single-crystal neutron diffraction study of natural chondrodite and clinohumites. Am Mineral 86:981–989

Friedrich A, Lager GA, Ulmer P, Kunz M, Marshall WG (2002) High-pressure single-crystal X-ray and powder neutron study of F, OH/OD-chondrodite: compressibility, structure, and hydrogen bonding. Am Mineral 87:931–939

Hamilton WC (1959) On the isotropic temperature factor equivalent to a given anisotropic temperature factor. Acta Crystallogr 12:609–610

Hawthorne FC (1992) The role of OH and H_2O in oxide and oxysalt minerals. Z. Kristallogr 201:183–206

Johnson CK (1970) The effect of thermal motion on interatomic distances and angles. Crystallographic Computing. In: Ahmed FR (ed) Munksgaard, Copenhagen, Denmark pp 220–226

Lager GA, Ulmer P, Miletich R, Marshall WG (2001) O-D···O bond geometry in OD-chondrodite. Am Mineral 86:176–180

Lehmann MS, Kuhs WF, McIntyre GJ, Wilkinson C, Allibon JR (1989) On the use of a small two-dimensional position-sensitive detector in neutron diffraction. J Appl Crystallogr 22:562–568

Libowitzky E (1999) Correlation of O-H stretching frequencies and O-H···O hydrogen bond lengths in minerals. Monatsh Chem 130:1047–1059

Liu L-G, Mernagh TP, Lin CC, Irifune T (1997) Raman spectra of phase E at various pressures and temperatures with geophysical implications. Earth Planet Sci Lett 149:57–65

Liu L-G, Lin CC, Mernagh TP, Irifune T (1998) Raman spectra of phase B at various pressures and temperatures. J Phys Chem Solids 59(6-7):871–877

Mernagh TP, Liu L-G, Lin CC (1999) Raman spectra of chondrodite at various temperatures. J Raman Spectrosc 30:963–969

Palmer DC (2003) CrystalMaker for Mac OS X, release 6.20. Bicester, UK

Shannon RD (1976) Revised effective ionic radii and systematic studies of interatomic distances in halides and chalcogenides. Acta Crystallogr A32:751–767

Sheldrick GM (1997) SHELXL-97—a program for crystal structure refinement. Release 97-2. University of Göttingen, Germany

Schomaker V, Trueblood KN (1998) Correlation of internal torsional motion with overall molecular motion in crystals. Acta Crystallogr B54:507–514

Stalder R, Ulmer P (2001) Phase relations of a serpentine composition between 5 and 14 GPa: significance of clinohumite and phase E as water carriers into the transition zone. Contrib Mineral Petrol 140(6):670–679

Wilkinson C, Khamis HW, Stansfield RFD, McIntyre GJ (1988) Integration of single-crystal reflections using area multidetectors. J Appl Crystallogr 21:471–578